Journal of Colloid and Interface Science 678 (2025) 1001–1011

Contents lists available at ScienceDirect

Journal of Colloid And Interface Science

journal homepage: www.elsevier.com/locate/jcis

Regular Article

The role of oleosins and phosphatidylcholines on the membrane mechanics of oleosomes

Jack Yang [a,b,1], Lorenz Plankensteiner [a,c,1], Anteun de Groot [b], Marie Hennebelle [c], Leonard M.C. Sagis [b], Constantinos V. Nikiforidis [a,*]

[a] Laboratory of Biobased Chemistry and Technology, Wageningen University, Bornse Weilanden 9, 6708WG Wageningen, The Netherlands
[b] Laboratory of Physics and Physical Chemistry of Foods, Wageningen University, Bornse Weilanden 9, 6708WG Wageningen, The Netherlands
[c] Laboratory of Food Chemistry, Wageningen University, Bornse Weilanden 9, 6708WG Wageningen, The Netherlands

GRAPHICAL ABSTRACT

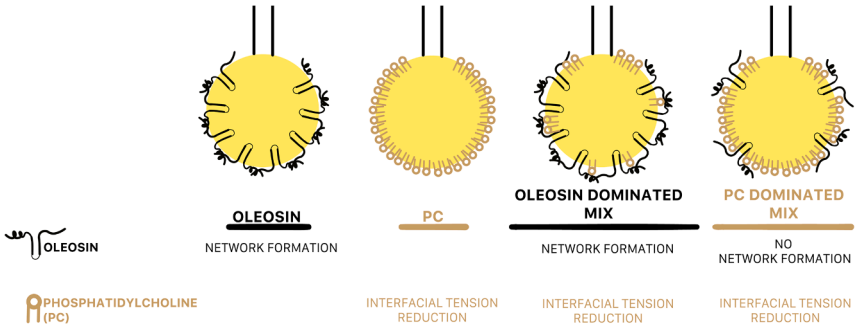

ARTICLE INFO

Keywords:
Lipid droplet
Phospholipid
Membrane protein
Surface dilatational rheology
General stress decomposition
Oil body

ABSTRACT

Hypothesis: Oilseeds use triacylglycerides as main energy source, and pack them into highly stable droplets (oleosomes) to facilitate the triacylglycerides' long-term storage in the aqueous cytosol. To prevent the coalescence of oleosomes, they are stabilized by a phospholipid monolayer and unique surfactant-shaped proteins, called oleosins. In this study, we use state-of-the-art interfacial techniques to reveal the function of each component at the oleosome interface.

Experiments: We created model oil–water interfaces with pure oleosins, phosphatidylcholines, or mixtures of both components (ratios of 3:1, 1:1, 1:3), and applied large oscillatory dilatational deformations (LAOD). The obtained rheological response was analyzed with general stress decomposition (GSD) to get insights into the role of phospholipids and oleosins on the mechanics of the interface.

Findings: Oleosins formed viscoelastic solid interfacial films due to network formation via in-plane interactions. Between adsorbed phosphatidylcholines, weak interactions were observed, suggesting the surface stress response upon dilatational deformations was dominated by density changes. In mixtures with 3:1 and 1:1 oleosin-to-phosphatidylcholine ratios, oleosins dominated the interfacial mechanics and formed a network, while phosphatidylcholines contributed to interfacial tension reduction. At higher phosphatidylcholine concentrations (1:3

* Corresponding author.
E-mail address: costas.nikiforidis@wur.nl (C.V. Nikiforidis).
[1] Co-first authors.

https://doi.org/10.1016/j.jcis.2024.09.171
Received 26 April 2024; Received in revised form 17 September 2024; Accepted 18 September 2024
Available online 19 September 2024
0021-9797/© 2024 The Author(s). Published by Elsevier Inc. This is an open access article under the CC BY license (http://creativecommons.org/licenses/by/4.0/).

oleosin-to-phosphatidylcholine), phosphatidylcholine dominated the interface, and no network formation occurred. Our findings improve the understanding of both components' role for oleosomes.

1. Introduction

The combination of phospholipids and proteins enables plants to successfully store water-insoluble triacylglycerides (TAGs) as oil droplets which are tightly packed in the aqueous cytosol. TAGs are stored in the core of specialized oil-storage organelles called oleosomes (lipid droplets or oil bodies) and are covered with a monolayer of phospholipids with embedded proteins, which kinetically stabilize the oil–water interface between the TAGs and the aqueous surroundings [1–3]. Particularly interesting is the stability of oleosomes in desiccation-tolerant (orthodox) seeds, as they can survive extreme environmental conditions and several years of storage without coalescing [4,5]. Due to this unique stability, oleosomes recently caught attention as an alternative to traditional emulsion droplets in food- and personal-care formulations [6,7]. Oleosomes are preferred over traditional emulsions as they are "natural" oil droplets that can be obtained by mild extraction from seeds, while traditional emulsion droplets are created through intensive processing from oil and emulsifiers [6]. Moreover, oleosomes high resistance to coalescence is maintained even at high temperatures [6–8]. Understanding the origins of oleosomes' physical stability will benefit the emerging interest in using oleosomes as it will help to ensure oleosomes' stability during processing and in applications. Additionally, the design principles of oleosomes could stimulate the creation of bio-inspired emulsion droplets with high physical stability.

Remarkably, a specific class of proteins with no known metabolic function makes up to 90 % of the total proteins in the oleosomes of desiccation-tolerant seeds [9–11]. These proteins are called oleosins and are suggested to have one single function: physically stabilizing oleosomes against coalescence [1,11–13]. Various *in vivo* and *in vitro* studies evidenced the oleosome stabilizing effect of oleosins [2,13–17]. The stabilizing role of oleosins against oleosome coalescence has been attributed to the structure of oleosins, which induces strong interactions with phospholipids on the oleosome interface [12,15,18].

Oleosins consist of a hydrophobic hairpin of ~72 residues that is attached to two mostly hydrophilic arms [10]. The most recent experimental and modeling data suggest that the hairpin consists of two alpha helixes that are connected via a proline knot, which forces a 180° turn, providing the hairpin-like structure [16,18,19]. The *N*-terminal arm is about ~30–50 residues long and was experimentally suggested to be mostly disordered with some beta sheet and alpha helix structure in *E. coli*-expressed sunflower oleosins [20]. The structure-predicting software Alpha Fold predicts the *N*-terminal arm to be completely disordered [18,21]. The C-terminal arm contains ~50–70 amino acids dependent on the oleosin isoform [9,22] and is predicted by Alpha Fold to be alpha-helical in the part of the arm adjacent to the hairpin and disordered at the end terminal [18,21]. From the primary sequence, the C-terminal arm appears to contain periodically spaced positively charged residues [9,18]. In the natural form of oleosomes, the hydrophobic hairpin is inserted into the TAG core of oleosomes, while the arms most likely face the aqueous bulk phase [2,12,23]. With its positively charged side groups, the arms are suggested to interact with phospholipids of the monolayer electrostatically, forming a rigid interfacial layer that was hypothesized to be the origin of the physical stability of oleosomes [15].

We recently observed that even in the absence of phospholipids, oleosins physically stabilized oil droplets [14]. Oleosins protected the droplets from coalescence and, when sufficiently charged (pH far from their isoelectric point), also from flocculation. These findings indicated that oleosins by themselves might be sufficient to physically stabilize oleosomes, e.g., they could form a solid-like interfacial layer similar to what is observed for other proteins [24,25]. This made us rethink the role of phospholipids in the physical stability of oleosomes. Possibly, the major role of phospholipids is to decrease the interfacial tension at the oil–water interface between oleosomes and the aqueous cytosol to reduce the free energy of the system [3,26]. For a mechanistic understanding of oleosomes' physical stability, it is essential to gain more insights into how oleosins contribute to the mechanics of the interfacial layer, and how they interact with phospholipids.

Dilatational rheology is a promising technique for studying the contribution of oleosins and phospholipids on the oleosome interface. Model oil–water interfaces with oleosins and phospholipids can be created and exposed to oscillatory deformation [27,28]. The rheological response to the deformation provides information on the mechanics of the oleosin and phospholipid stabilized oil–water interface, which gives insights into the role of oleosins and the intermolecular interactions between the oleosins and phospholipids [27,29]. The standard analyses are performed at small deformations, typically < 10 % amplitude [15], while at larger deformations, additional non-linear rheological responses are generated due to the alteration of the interfacial microstructure. This deformation region with highly non-linear rheological responses is often referred to as the non-linear viscoelastic (NLVE) regime [28]. A challenge of measuring in the NLVE regime is the inaccuracy of the commonly used first-harmonic-based surface dilatational moduli (E_d), as the E_d does not fully capture the generated non-linearities. Accurate measurements in the NLVE regime would facilitate new insights into the intermolecular interactions between oleosins and phospholipids at the oleosome interface.

In this work, we dive into the non-linear contributions of rapeseed oleosins and the main phospholipid phosphatidylcholine (~60 % of the phospholipids in rapeseed oleosomes [30]) at oil–water interfacial films to obtain a deeper understanding of the mechanical properties of the oleosome membrane. We combine large amplitude dilatational oscillatory (LAOD) rheology with general stress decomposition (GSD), a new method developed by de Groot, et al. [28] to quantitatively analyze the NLVE regime. Especially, the quantification of non-linearities in dilatational rheology remained challenging in the past, due to the generation of density-generated even harmonics in the Fourier spectrum. The GSD allows us to separate both odd and even harmonics, and, thus, the quantification of the non-linearities in LAOD. Our findings illustrate how state-of-the-art interfacial science sheds light on the functions of oleosins and phosphatidylcholines on the mechanical properties of the oleosome membrane, and, thus, the potential of the presented toolset in studying mechanical properties of biological interfacial films. We studied different oleosin:phosphatidylcholine ratios to gain a mechanistic understanding of nature's choice when designing oleosomes. Understanding the design principles of oleosomes might allow to create bio-inspired droplets with uniquely high physical stability.

2. Experimental section

2.1. Materials

The used rapeseeds (*Brassica napus*) of the variety Alizze were obtained from a European seed producer and kept at −20 °C. Soy Phosphatidylcholine (PC) was purchased from Avanti Polar Lipids Inc. (Alabama, USA) and stored at −20 °C. The rapeseed oil was obtained by Danone Nutricia Research (The Netherlands) and also stored at −20 °C. All used solvents were bought from Biosolve (The Netherlands). All other chemicals were obtained from Merck (Germany). All experiments were performed with Ultrapure water (MilliQ Purelab Ultra, Germany).

2.2. Sample preparation

2.2.1. Isolation of oleosins (OL)

A schematic overview of the overall experimental approach is shown in Fig. 1. Oleosins (OL) were obtained with a recently published extraction method [31]. Rapeseeds were mixed with 0.1 M $NaHCO_3$ at pH 9.5 in a 1:7 (w:w) seed-to-buffer ratio and soaked at 4 °C for 16 h. The soaked seeds were blended in a blender (Waring Commercial 7011HS, Wyoming, USA) for 2 min at maximum speed. After blending the mix was filtered with cheesecloth and a vacuum pump. The obtained filtrate was centrifuged at a speed of 10,000xg for 30 min at 4 °C. The top layer was collected and redispersed in 0.1 M $NaHCO_3$ (pH 9.5) at a 1:4 (w:w) cream-to-buffer ratio to wash the oleosome cream. Then, the centrifugation and collection steps were repeated. These washing steps were repeated once more using water instead of the 0.1 M $NaHCO_3$. The final cream layer was collected as purified oleosomes and stored at −30 °C for following OL extraction.

Thawed oleosome cream was combined with methanol in a ratio of 1:2 w/v. The mix was incubated for 10 min at room temperature. After incubation, the mixture was centrifuged at 4,700xg for 10 min. The top methanol phase was discarded, and the pellet was collected. The same methanol washing steps were repeated on the pellet three more times. Then, the same washing steps were performed four times with hexane and three additional times with ethanol. The obtained pellet was dispersed in 10 mL water with the help of a sonication bath running at 40 kHz (M2800, Branson, Missouri, USA) for 5 min. The OL-water solution was freeze-dried to collect the extracted OL. The OL extract was devoid of other proteins and had a purity of 88.4 % as described in [14]. Only a minor contamination of 1–2 wt% of phosphatidylinositol (PI) was detected [14]. The OL extract was stored at −30 °C.

We confirmed in our previous work that the extracted oleosins can be used to create oleosome model systems [14]. The microstructure and interfacial oleosin load were almost identical for model droplets stabilized by extracted oleosins and native oleosomes [14]. The results made us confident to use the isolated oleosins to create the model interfaces in this study. Nevertheless, we are aware that the structure of oleosins might undergo some structural changes during the extraction procedure.

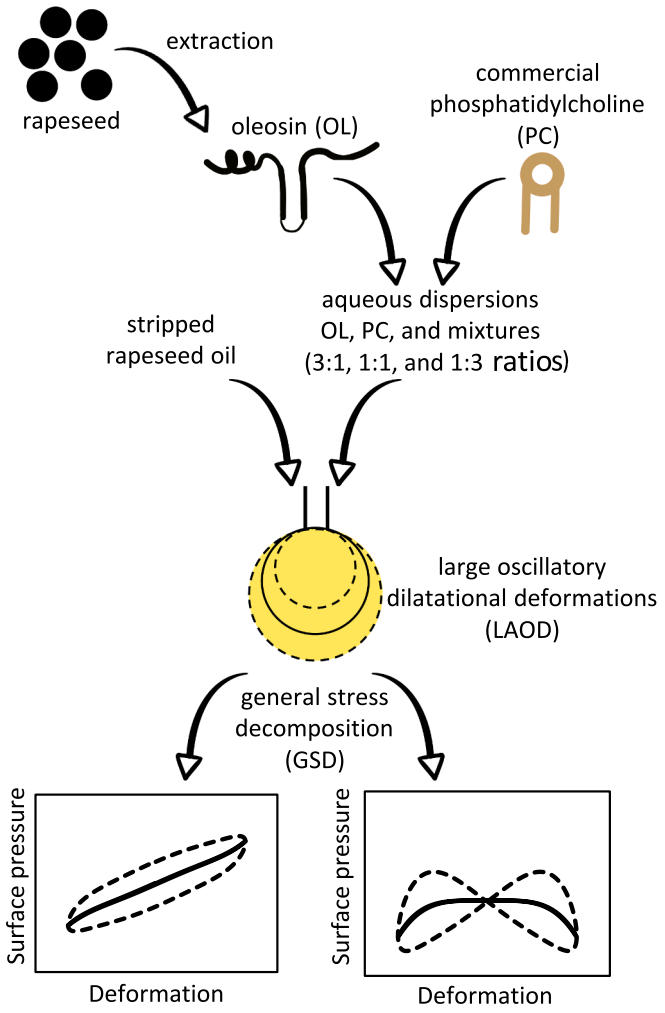

Fig. 1. Schematic overview of the experimental approach in this work.

2.2.2. Preparation of OL and phosphatidylcholine (PC) solutions

PC solutions were prepared at concentrations of 1 g/L in 10 mM phosphate buffer (30 mM ionic strength) at pH 8.0. The tubes were covered with aluminum foil to avoid light oxidation and mixed in an overhead tube rotator for 4 h at room temperature. Afterwards, the solutions were sonicated in a sonication bath running (40 kHz) for 10 min.

OL solutions were also prepared at 1 g/L with the same steps as for the PC solutions. Then, the OL solutions were filtered using a 0.45 μm syringe filter (Minisart® Cellulose-Acetate, Sartorius, Germany), resulting in a filtrate with a concentration of 0.1 g/L, as confirmed with the Pierce™ BCA protein assay kit (Thermo Scientific, Massachusetts, USA).

The PC and OL solutions were then diluted to reach concentrations of 0.02 g/L. The two compounds were studied individually or mixed at a 1:3, 1:1, and 3:1 (w:w) OL-to-PC ratio. The ratios were based on the typical range of ratios found in oleosomes, which is between 1:1 and 3:1 OL-to-phospholipid ratio [32]. We want to highlight that the OL-to-PC ratios in the bulk solution do not necessarily reflect the ratio on the interface. Both components will compete for adsorption to the oil–water interface. Nevertheless, our goal was to create interfacial films with varying contents of both components to test each component's influence on the interfacial mechanics. We successfully achieved this goal as evidenced from the data in section 3.1. For the mixtures, the OL concentration was always fixed at 0.02 g/L, while the PC concentration was varied. The concentration ranges in the study were chosen to enable the dilatational rheology measurements. Preliminary experiments showed that higher concentrations lead to too-low surface tensions and the droplet detaches already at small deformations. All solutions were stored in the fridge and used within 24 h after preparation.

2.2.3. Oil stripping

Surface active impurities were removed from rapeseed oil by mixing oil with Florisil (100–200 mesh, magnesium silicate, Sigma-Aldrich, Missouri, USA) at a Florisil-to-oil ratio of 1:2 (v/v). The mixture was transferred into tubes covered in aluminum foil to prevent photooxidation. The tubes were mixed overnight in an overhead rotator at room temperature. The mix was then centrifuged thrice at 2,000xg for 20 min to remove the Florisil. The stripped oil was stored at −20 °C.

2.3. Surface dilatational rheology

The rheological properties of the interface were studied with an automated drop tensiometer (ADT, Teclis, France) (Fig. 1). A hanging droplet (area of 20 mm^2) of OL/PC solution was created at the tip of a (G18) needle in stripped rapeseed oil. The interfacial tension was determined by monitoring the droplet with a camera and fitting its shape to the Young-Laplace equation. We decided to deliver both OL and PC to the interface via the water phase. Thereby, we could ensure a clear oil phase and droplet shape for proper image analysis. Moreover, oleosins' delivery through the water phase was in line with our previous work that showed that isolated oleosins can be used to create oleosome model systems. The interfacial tension of an oil–water interface (without OL or PC) was stable at 29.2 ± 0.2 mN/m. For the first two hours, the droplet area was maintained constant to observe the adsorption of OL and PC. Then, the area was changed with either an amplitude or frequency

sweep. The two-hour waiting time was chosen, as we obtained a near constant surface pressure, which increases the quality of the deformations and surface stress output. The amplitude sweep was performed with 2.5 – 50 % area deformation with a constant frequency of 0.02 Hz. The frequency sweep was performed with a fixed area deformation of 5 %, with frequencies increasing from 0.005 to 0.1 Hz. At each deformation amplitude or frequency step, five oscillatory cycles were performed with a pause length similar to one oscillation cycle between each deformation step. All experiments were performed in triplicate at 20 °C.

2.4. Analyzing non-linearities with Lissajous plots and general stress decomposition

The stress response of the amplitude sweeps was quantified by the decomposition of the surface stress in odd and even harmonics with the general stress decomposition (GSD) (Fig. 1) developed by de Groot, et al. [28] in MATLAB (2022b). GSD was applied to the middle three oscillations to exclude artifacts from the sweep start and stop. The stress response was first analyzed with a Fourier transform. Higher harmonics (I_n) from the Fourier transform were included when their relative contribution was at least 3 % compared to the first harmonic intensity (I_1), i.e., $I_n/I_1 > 0.03$. The resulting harmonics were then used to reconstruct the separate contribution of the odd (equation (1) and even harmonics (equation (2):

$$\Pi(t)_{odd} = \tau_1 + \tau_2 = \sum_{k=0}^{\frac{m}{2}} b'_{2k+1} sin((2k+1)\omega t) + \sum_{k=0}^{\frac{m}{2}} a'_{2k+1} cos((2k+1)\omega t) \quad (1)$$

$$\Pi(t)_{even} = \tau_3 + \tau_4 = \sum_{k=0}^{\frac{m}{2}} c'_{2k} sin(2k\omega t) + \sum_{k=0}^{\frac{m}{2}} d'_{2k} cos(2k\omega t) \quad (2)$$

Here, ω is the frequency of deformation, t is the time, and m is the highest included harmonic. The odd harmonics consisted of τ_1 and τ_2, which are the elastic and viscous contributions of the network response with Fourier coefficients b'_{2k+1} and a'_{2k+1}. The even harmonics consisted of τ_3 and τ_4, which are the viscous and elastic contribution of the non-linearities in the surface density changes with Fourier coefficients c'_{2k} and d'_{2k}. Based on the equations of odd and even harmonics, characteristic properties of the stress response were quantified by equations 3–7:

$$E_{\tau 1L} = \frac{\sum_{k=0}^{m} b'_{2k+1}(-1)^k}{\varepsilon_0} \quad (3)$$

$$E_{\tau 1M} = \frac{\sum_{k=0}^{m} (2k+1) b'_{2k+1}}{\varepsilon_0} \quad (4)$$

$$S = \frac{E_{\tau 1L} - E_{\tau 1M}}{E_{\tau 1L}} \quad (5)$$

$$E_{\tau 4} = -\frac{\sum_{k=0}^{m} 2d'_{4k+2}}{\varepsilon_0} \quad (6)$$

$$U_{d\tau 2} = \pi \varepsilon_0^2 E''_1 \quad (7)$$

Here, ε_0 is the strain amplitude of the applied deformation ($\varepsilon = \varepsilon_0 \sin(\omega t)$), E''_1 is the loss modulus of the first harmonic, and $E_{2k\tau 3}$ is the modulus of each harmonic contained in τ_3. $E_{\tau 1L}$ and $E_{\tau 1M}$ describe the secant elastic modulus at maximum strain and elastic modulus at zero strain of the odd harmonics. The factor S calculated from $E_{\tau 1L}$ and $E_{\tau 1M}$ describes the intracycle strain stiffening or softening. Intracycle viscous dissipation of the odd harmonics is described by $U_{d\tau 2}$. Even harmonics are further quantified by the elastic modulus $E_{\tau 4}$.

Each of the aforementioned parameters can be shown in a Lissajous plot, for a visualization, we refer to de Groot, et al. [28]. Lissajous plots were constructed by plotting the surface pressure $\Pi = \gamma\text{-}\gamma_0$ versus the deformation $(A\text{-}A_0)/A_0$, where γ and A are the surface tension and area of the droplet's deformed interface, and γ_0 and A_0 are the surface tension and area of the non-deformed interface, respectively.

3. Results and discussion

3.1. Adsorption to the oil–water interface

To study the dilatational rheology of oleosins (OL), phosphatidylcholine (PC), and their mixtures, we used automated drop tensiometry (ADT). The adsorption to the oil–water interface in the ADT setup is influenced by diffusion from bulk to the interface, intermolecular interactions, and interfacial properties [33,34]. Due to the complexity of the adsorption process, it was not possible to exactly control the interfacial concentration of each component in the mixtures. Therefore, we controlled the concentration of OL and PC in the bulk phase to obtain interfaces with varying contents of each component. We confirmed the success of our strategy by comparing the interfacial adsorption and interfacial properties of the mixtures to the individual compounds as described in the following sections. The adsorption of OL alone (0.02 g/L) is plotted in Fig. 2A-C as a reference. OL showed a lag phase of 10 s before adsorbing to the interface. Then, the surface pressure increased to 10.1 mN/m after 2 h of adsorption time (Fig. 2A-C).

For PC, three concentrations were studied: 0.0066 g/L (Fig. 2A), 0.02 g/L (Fig. 2B), and 0.06 g/L (Fig. 2C) corresponding to the PC concentration in the OL-PC mixtures with a 3:1, 1:1, and 1:3 OL:PC (w:w) ratio. The adsorption behavior of PC was concentration dependent. At 0.0066 g/L (Fig. 2A), a lag phase of 135 s was present, followed by an increase to 10.8 mN/m after 2 h. Increasing the PC concentration to 0.02 g/L led to an immediate slow increase of the surface pressure, which then rapidly increased after 100 s to reach a surface pressure of 12.8 mN/m after 2 h (Fig. 2B). When 0.06 g/L PC were used, an immediate jump to a surface pressure of 2.3 mN/m occurred, followed by a further increase to 14.5 mN/m after 2 h (Fig. 2C).

The 3:1 OL-PC mixture followed the same adsorption behavior as the pure OL (Fig. 2A), indicating that OL primarily adsorbed in this mixture. Moreover, it indicated that a possible interaction of PC and OL in the bulk did not influence the adsorption dynamics. The comparison of the adsorption of the pure PC at a concentration of 0.0066 g/L and the pure OL confirmed the slightly higher surface activity of OL at these concentrations (Fig. 2A). When OL and PC were mixed in a 1:1 ratio, the mixture behaved as an intermediate between pure PC at 0.02 g/L and pure OL (Fig. 2B), which suggested the co-adsorption of both components. Similarly, the obtained adsorption curve for the 1:3 OL-PC indicated co-adsorption of OL and PC to the oil–water interface, as even higher surface pressures were reached than for the individual OL or PC (Fig. 2C). The surface pressure increased immediately to 3.6 mN/m and then reached 15.3 mN/m after 2 h. In summary, when more OL was present than PC (3:1 OL-PC mixture), OL seemed to dominate the adsorption behavior, while increasing the PC concentration to a 1:1 OL-PC ratio led to a more PC-dominated adsorption behavior. The mixture with a 1:3 OL-PC ratio showed a synergy, the surface pressure increased faster than for each individual component. The adsorption results indicated that we successfully obtained mixed interfaces with varying contents of OL and PC by controlling their concentrations in the bulk.

The fairly similar adsorption behavior of OL and PC might have derived from the structures they form in aqueous dispersions; both are present as larger assemblies [14,35–37]. Oleosins are reported to self-assemble into micelle-like particles of ~30 nm due to their surfactant-like structure [14,38,39]. These particles can further cluster into larger aggregates, which probably were in the size range of 50–400 nm after the applied filtration [14]. PC is most likely assembled into lamellar phases that are associated into larger structures [35–37]. Both the OL and PC assemblies should rupture and spread on the oil–water interface before adsorbing [14,40]. The sudden introduction of surface-

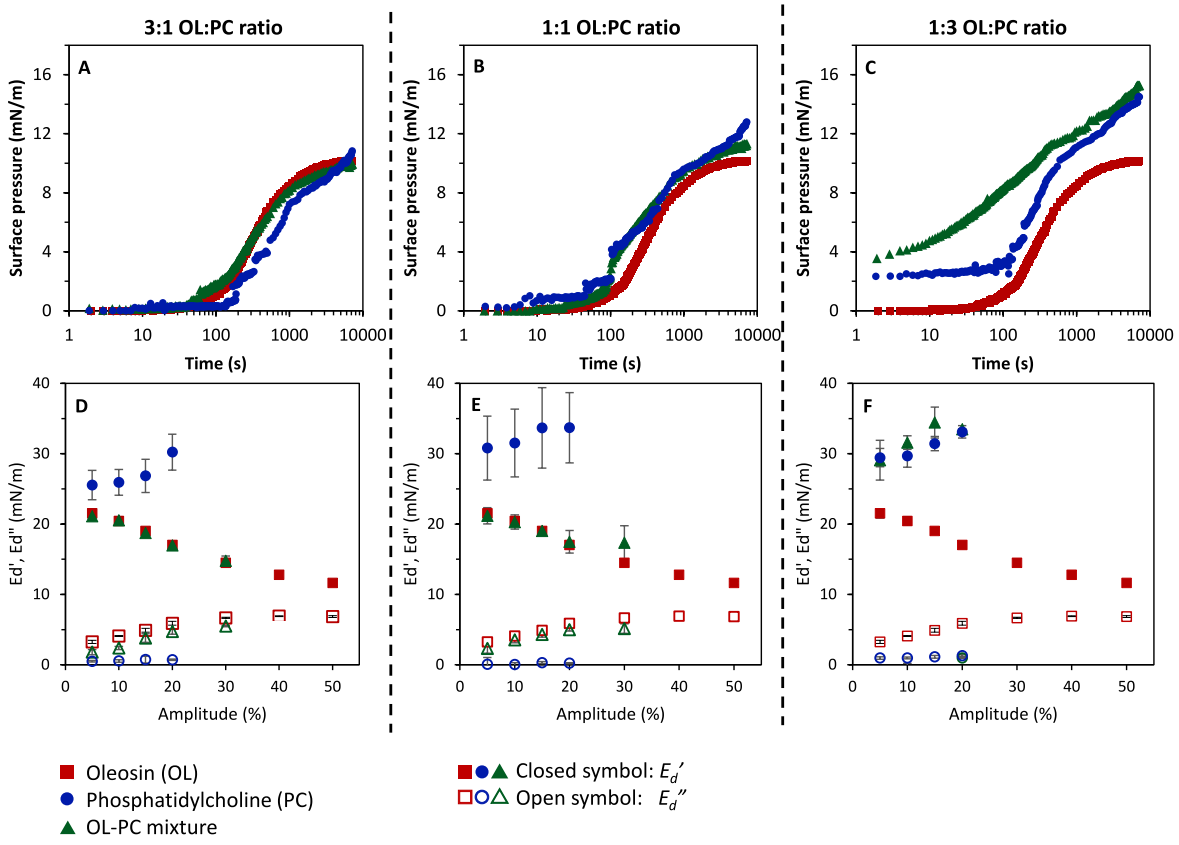

Fig. 2. Panels A-C) Surface pressure as a function of time for the oil–water interfaces stabilized by OL (oleosin), PC (phosphatidylcholine), and the OL-PC mixtures. We studied three ratios for the OL and PC mixtures: 1:3 (A), 1:1 (B), and 3:1 (C) OL:PC. The plots for pure OL and pure PC are presented as references in each plot. The oleosin concentration was fixed at 0.02 g/L, while the PC concentration was varied from 0.0066 g/L, 0.02 g/l and 0.06 g/L. All samples were prepared in 10 mM phosphate buffer at pH 8.0. After 2 h of adsorption, the obtained interfaces were subjected to surface dilatational rheology. Panels D-F) Surface dilatational moduli as a function of amplitude. Here, E_d' is the elastic component, and E_d" is the viscous component of the modulus.

active molecules could lead to a rapid increase of the surface pressure, as we observed for the 3:1 OL-PC mixture where the surface pressure increased stepwise between 180 to 600 s and the 1:1 OL-PC mixture where a similar stepwise increase occurred around 100 s.

3.2. Surface dilatational rheology

After the 2 h of adsorption, the mechanical properties of the oil–water interface were characterized using surface dilatational rheology. An amplitude sweep with deformations increasing from 5 to 50 % was applied. The obtained rheological response was first analyzed classically using the first harmonic-based surface dilatational moduli described in section 3.2.1. and then by also considering non-linearities as described in sections 3.2.2. and 3.2.3..

3.2.1. First harmonic-based analysis of the rheological response

For OL (Fig. 2D-F), we observed a surface elastic dilatational modulus (E_d') of 21.5 mN/m at 5 % deformation, which decreased to 11.6 mN/m at 50 % deformation. The presence of a surface viscous dilatational modulus (E_d") of the OL-stabilized interface suggested an overall viscoelastic behavior. The PC at all three concentrations (Fig. 2D-F) showed similar behavior for the E_d', which slowly increased from 25 to 31 mN/m at 5 % deformation to 31–34 mN/m at 20 % deformation. At > 20 % deformation, the oil droplet detached from the needle during the compression cycle, as the surface tension reached near zero values. The E_d"-values for PC were close to zero (<1 mN/m), suggesting an almost fully elastic response.

The 3:1 OL-PC mixture had an E_d' of 21.1 mN/m at 5 % deformation and decreased to 14.8 mN/m at 30 % deformation (Fig. 2D). Again, the droplet detached at high deformations (>30 %) due to gravity overcoming the extremely low surface tension. The amplitude-dependent changes of the moduli for this mixture were very similar to those of the pure OL-stabilized interface, which suggested that OL dominated the mechanics of the interface and was responsible for the viscoelastic behavior. These findings aligned with this mixture's adsorption isotherm, suggesting OL's dominance (Fig. 2A). However, the rheology results highlighted that PC also played a role in the mixture, as the droplet detached at deformations above 30 %, which was not the case for the purely OL-stabilized interface. PC likely adsorbed to the interface and contributed to further reduction of the interfacial tension leading to the droplet detachment.

Similarly, the moduli for the 1:1 OL-PC mixture followed the amplitude dependence of the pure OL-interface, with droplet detachment at higher deformations than 30 %. Also, for this mixing ratio, OL seemed to dominate the mechanical properties, and PC further decreased the interfacial tension, leading to droplet detachment. When the concentration of PC was further increased to reach the 1:3 ratio of OL:PC, the moduli shifted to be more like the ones of pure PC (Fig. 2F). Therefore, PC dominated the oil–water interface at such a high PC concentration. The first harmonic-based analysis further confirmed that we successfully created mixed interfaces with varying contents of OL and PC in line with the adsorption results.

Unexpectedly, the interfaces solely stabilized by PC and the PC-dominant 1:3 OL-PC mixture had higher E_d' than those stabilized by pure OL and the OL-dominant mixtures. Similar observations were made by Deleu, et al. [15] when using rapeseed OL and a mixture of phospholipids to stabilize triolein-water interfaces. To better understand the high E_d'-values of PC and the 1:3 OL-PC mixture, we performed so-called

frequency sweeps, where the oscillatory frequency was incremented from 0.005 to 0.1 Hz at a fixed deformation. The dependence of the frequency was quantified using a power-law scaling, $E_d' \sim \omega^n$. For surfactants with little to no in-plane interactions at the interface, the interfacial elasticity is predominantly affected by the molecular exchange between the bulk phase and the interface. According to the Lucassen-van den Tempel model, this should lead to a n-value of 0.5. The purely PC-stabilized interfaces had an n-value of 0.03 ± 0.02, and the purely OL-stabilized ones had a n-value of 0.04 ± 0.03. The low n-value for OL aligned with the n-values reported for other protein-stabilized interfaces, for which n-values are often close to zero due to strong in-plane interactions at the interface [41,42]. However, the similarly low n-value for the PC-stabilized interfaces was surprising, as very weak in-plane interactions were expected, especially as this interface showed a fully elastic response similar to a previously reported phospholipid-stabilized air–water interface [42]. This low n-value might indicate that in the applied frequency range, the compression and expansion rate of the interface is substantially faster than the adsorption/desorption rate of the phospholipids. As a result, there is no phospholipid exchange between bulk and interface. The surface density changes during oscillations, resulting in substantial surface pressure changes and the high E_d'-values.

Therefore, the results should be interpreted carefully. The higher E_d'-values of the PC stabilized interfaces do not directly mean that PC formed stiffer interfaces than OL. Here, a direct comparison between the PC and OL-stabilized interfaces based on the first harmonic-based analysis might be inaccurate. The E_d' of OL and OL dominant OL-PC mixtures decreased with increasing deformation amplitude, suggesting that the measurements are in the non-linear viscoelastic (NLVE) regime [28]. In the NLVE regime, the first harmonic-based analysis does not fully capture the interfacial phenomena [28]. In this regime, higher harmonics are generated, which are not included in the calculation of the first harmonic-based moduli [27,28]. In the next sections, we used Lissajous plots and general stress decomposition (GSD) to qualitatively and quantitatively analyze these non-linearities.

3.2.2. *Analysis of non-linearities using Lissajous plots*

The non-linearities in the rheological response of the OL-PC

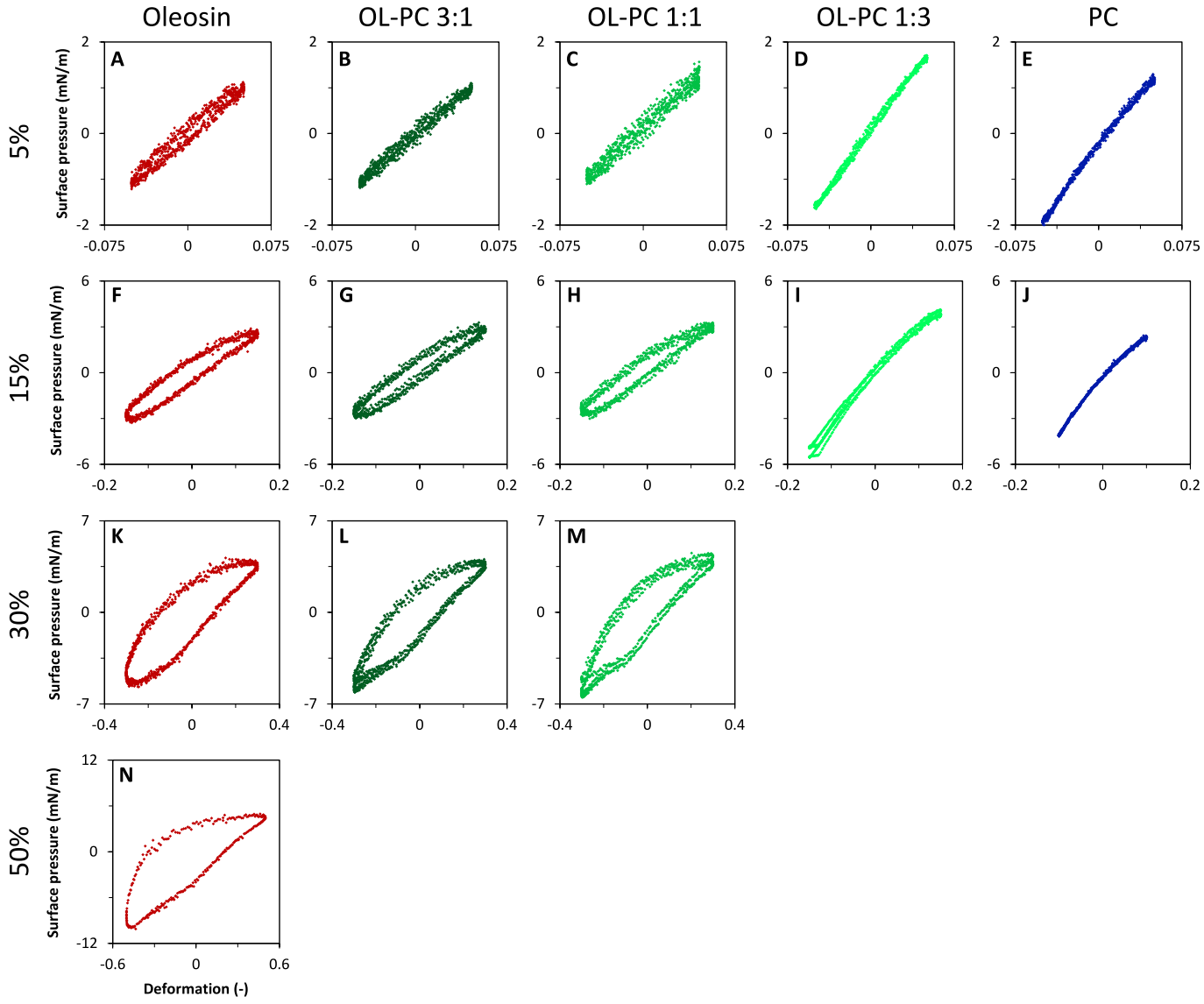

Fig. 3. Lissajous plots of the surface pressure as a function of the deformation. The data was obtained from amplitude sweeps of interfaces stabilized by oleosins (OL), phosphatidylcholine (PC), and OL-PC mixtures. The ratios of OL to PC are shown above the plots as w:w ratio. The OL concentration in all samples was fixed at 0.02 g/L. The PC concentration of the pure PC sample shown in panels E and J was also at 0.02 g/L, while the PC concentration in the mixtures varied from 0.0066 g/L, 0.02 g/l and 0.06 g/L. All samples were prepared in 10 mM phosphate buffer at pH 8.

interfaces were quantitatively analyzed with Lissajous(−Bowditch) plots of the surface stress over deformation (Fig. 3). In general, Lissajous plots follow a clockwise pattern with the upper part of the loop representing the expansion and the bottom part the compression of the interfacial area. The shape of the Lissajous plots gives insight into the rheological response; a fully elastic response of the interface leads to a closed plot (a straight line), while a fully viscous response leads to an open circle. An intermediate elliptical shape, thus, represents a combination of both and indicates a viscoelastic response to deformation. Asymmetry between the expansion and compression part points to a non-linear rheological response of the interfacial layer. For more extensive explanations of the use of Lissajous plots in non-linear rheology, we refer to previous works [28,43,44].

The 5 % deformation Lissajous plot of the OL-stabilized oil–water interface (Fig. 3A) was a nearly closed ellipse, which suggested a predominantly elastic response of the OL interface. With increasing deformations, the plots widened, and pronounced asymmetries appeared (Fig. 3F, K, and N). Particularly, at 30 and 50 % deformation (Fig. 3K and N), the response differed largely when comparing the expansion and compression part of the plots. At 50 % deformation (Fig. 3N), the surface pressure increased steeply at the start of the expansion (lower left corner), and then the slope of the curve decreased towards maximum expansion (upper right corner). This is a typical pattern for interfaces that undergo strain-softening in expansion. In the compression cycle, the surface pressure decreased rapidly until the minimal surface pressure at maximum compression and showed a mild strain hardening in compression. Similar asymmetric behavior was previously shown for whey protein isolates, of which one of the main proteins is beta-lactoglobulin, and that is suggested to form a solid-like interfacial layer via a network formed by intermolecular interactions [25,42,45]. The similarity in the rheological response indicated that the adsorbed OL molecules might also interact intermolecularly, leading to a viscoelastic solid interfacial layer. The interactions between OL are most likely of non-covalent origin, as rapeseed oleosins lack cysteines, which could form covalent interactions via disulfide bonds [9]. The possible driving forces of the intermolecular interactions are discussed in more detail in section 3.3. During the expansive deformation of the interface, the interactions appeared to rupture, leading to the strain-softening behavior.

The interfaces stabilized purely by PC gave fully closed Lissajous plots (Fig. 3E and J), independent of whether the interfaces were deformed by an amplitude of 5 % or 15 %. The closed plots suggested a fully elastic response, which was in line with the near zero viscous modulus E_d" reported in Fig. 2D-F. The fully elastic PC response was independent of the deformation amplitude, indicating weak interactions between the adsorbed PC molecules on the interface.

The Lissajous plots for the 3:1 and 1:1 OL-PC mixture-stabilized interfacial films were almost identical to the ones of the pure OL stabilized interface at 5 % (Fig. 3A-C) and 15 % (Fig. 3F-H) deformation, once more highlighting the dominance of OL for the interfacial rheology in these mixtures. At a larger deformation of 30 % (Fig. 3L and M), the plots started to show a slight flattening at the end of the compression cycle (lower left corner), indicating strain softening in compression. The softening could be a contribution from the PC, as similar softening was previously reported for rapeseed lecithin (a mix of phospholipids) at the air–water interface [42]. The interfaces stabilized with the 1:3 OL-PC mixture gave fully closed Lissajous plots (Fig. 3D and I), similar to pure PC (Fig. 3E and J). In line with the previously described findings, this rheological behavior implied the dominance of PC in the interface's rheology of the 1:3 OL-PC mixture.

Before discussing the contribution of OL and PC further, general stress decomposition (GSD) was performed on the raw stress output to gain more insights into the interfaces' asymmetric rheological behavior.

3.2.3. General stress decomposition (GSD) – Lissajous plots

During the expansions and compressions of the surface area in dilatational deformation, the surface density changes. Hence, the non-linear rheological behavior of the OL- and the OL-PC mixture-stabilized interfacial films can originate from network interactions or surface density changes. Due to the presence of these surface density changes, the spectrum of a Fourier transformation of the stress signal will have both odd and even harmonics, which is in contrast to shear rheology, where only odd harmonics appear. In Lissajous plots, odd and even harmonics are not distinguishable. In contrast with the GSD, the stress signal can be split into the odd harmonics, which mostly represent network interactions, and the even harmonics, which derive from the density changes upon deformation [28,43].

As both odd and even harmonics have an energy storing (elastic) and energy dissipating (viscous) component, four basic stresses were obtained with the GSD: τ_1 representing the elastic component of the odd harmonics, τ_2 representing the viscous component of the odd harmonics, and τ_4 and τ_3 representing the elastic and viscous component of the even harmonics, respectively. The parameters were then plotted over deformation to construct new Lissajous plots and are presented in Fig. 4 for OL- and PC-stabilized interfaces. We focused here on the interface of the pure components to highlight the different behaviors. The Lissajous plots of the mixtures are shown in Figure S1 in the supplementary material. Two types of plots are shown in Fig. 4: 1) the combined signal of the odd harmonics ($\tau_1 + \tau_2$) and the elastic component (τ_1) in Fig. 4A-D and I-J, and 2) the combined signal of the even harmonics ($\tau_3 + \tau_4$) and the elastic component ($\tau 4$) in Fig. 4E-H and K-L.

The OL-stabilized interface gave a very narrow $\tau_1 + \tau_2$ curve and a straight τ_1 curve at 5 % deformation (Fig. 4A), again suggesting a predominant linear elastic response. At higher deformations (Fig. 4B-D), the $\tau_1 + \tau_2$ plot started to widen, suggesting a stronger contribution of the viscous component due to higher energy dissipation. At 50 % deformation (Fig. 4D), a rhomboidal shape emerged for $\tau_1 + \tau_2$, and the τ_1 curve (Fig. 4D) started to show a slight non-linearity with minor strain hardening at the extremes of the deformation curve (−0.5 or 0.5). This shape was likely the result of intra-cycle yielding. Such a behavior is often seen for gel-like systems in bulk shear rheology and surface shear rheology, and further supports the previous indication that adsorbed OL formed an intermolecular network due to attractive forces [43,46]. At 5 and 15 % deformation, the odd harmonics (Fig. 4A and B) dominated the signal over the even harmonics (Fig. 4E and F), which suggests that the signal came predominantly from the network interactions. At higher deformations (Fig. 4G and H), the even harmonics' signal increased, indicating a larger contribution by the density changes. This possibly resulted from extensive network disruption at such a high deformation.

In contrast, the τ_1 and $\tau_1 + \tau_2$ plots for the PC-stabilized interface were almost a straight line (Fig. 4I and J). The overlapping of the τ_1 and $\tau_1 + \tau_2$ curves suggested a fully elastically dominated response with no energy dissipation, indicating the in-plane interactions at the interface are too weak to result in any significant degree of network formation. The PC-stabilized interface had a large contribution of $\tau_3 + \tau_4$ (Fig. 4K and L), where the elastic component τ_4 almost fully dominated the signal from the even harmonics. The contribution of even harmonics, and thus the contribution resulting from density changes, were larger for the PC-stabilized interface than for the OL-stabilized one.

3.2.4. General stress decomposition – Quantification

Based on the GSD analysis, we then quantified the non-linearities in the stress signals for the OL-, PC- and OL-PC mixture-stabilized interfaces. With the odd harmonics, we calculated the elastic modulus $E_{\tau 1m}$ from the slope of τ_1 at zero strain (Fig. 5A). The viscous energy dissipation $U_{d\tau 2}$ was calculated from the area of τ_2 (Fig. 5B), and a stiffening value (S-value) was also obtained from τ_1 (Fig. 5D) [28]. From the even harmonics, we calculated the elastic modulus $E_{\tau 4}$, which is the secant modulus of τ_4 at maximum strain (Fig. 5C).

The $E_{\tau 1m}$ for the OL-stabilized interface decreased with increasing deformation (Fig. 5A). Simultaneously, the dissipated energy $U_{d\tau 2}$ increased, and the density contribution $E_{\tau 4}$ stayed close to 0. Combined, these observations suggested once more the formation of a solid-like

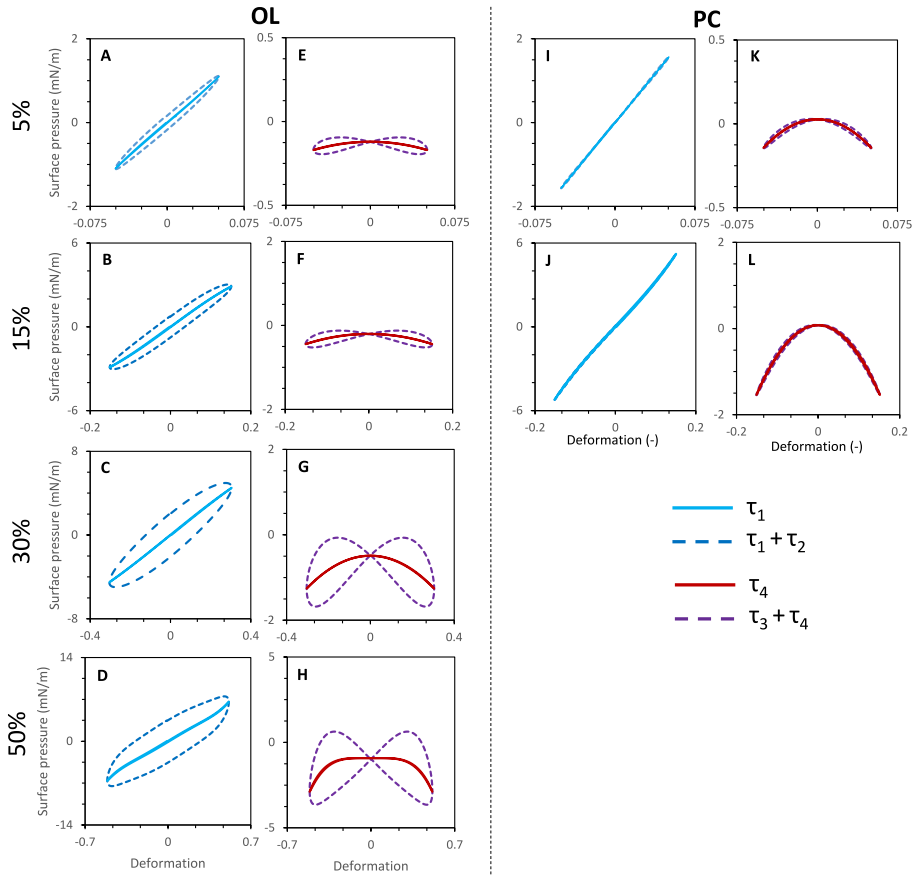

Fig. 4. Lissajous plots of surface pressure as a function of deformation for the four parameters obtained by splitting the surface stress signal with the general stress decomposition (GSD). The signal was decomposed into the components τ_1 and τ_2 representing the elastic and viscous component of the odd harmonics, and τ_4 and τ_3 representing the elastic and viscous component of the even harmonics. The plots are obtained from amplitude sweeps, as shown in Fig. 3. Panels A-H show the plots for the purely oleosin-stabilized (OL) interface and panels I-L for the purely phosphatidylcholine-stabilized (PC) interface.

network at the interface. For the PC-stabilized interface, a fully elastic response was obtained with a high $E_{\tau 1m}$ and no energy dissipation ($U_{d\tau 2}$). The high $E_{\tau 4}$ indicated a large contribution of density changes upon deformation, which was in stark contrast to the OL-stabilized interface. The PC-stabilized interface is elastic, with little to no in-plane network interactions among adsorbed molecules. Phospholipids are known to have complex phase diagrams, especially at higher compressions, where the interface can transition from a gas phase to a liquid-expanded, liquid-condensed and condensed/solid phase, with different orientations of the phospholipid tails towards the hydrophobic phase [40]. Especially at extreme compressions, the condensed phase might exist as a glass-like structure, potentially explaining the high contribution of $E_{\tau 4}$ for PC at higher deformations.

For the 3:1 and 1:1 OL-PC mixtures, the $E_{\tau 1m}$ was similar to that of pure OL. Also, the $U_{d\tau 2}$ followed the increase of pure OL, but slightly less energy dissipation occurred at 30 % deformation. Additionally, the mixtures had slightly more negative $E_{\tau 4}$ than the pure OL. The interfaces stabilized by the 3:1 and 1:1 OL-PC mixtures were hence dominated by network interactions and had only minor contributions from the density changes. The presence of PC led to slightly larger density contributions and less dissipated energy at deformations $>$ 20 % compared to the purely OL-stabilized interface.

By further increasing the amount of PC to a 1:3 OL-PC mixture, all values started to nearly overlap with those of pure PC. The OL still had a minor contribution, as it might have increased the $E_{\tau 4}$, suggesting a lower contribution of the surface density, while also shifting the S-value slightly to pure OL.

In summary, the dilatational rheology experiments revealed that the stress response of the OL-dominated interfaces (pure OL-stabilized interface, 3:1 and 1:1 OL-PC mixtures) was mostly linear elastic at small deformations (up to 15 % area change) with main contributions of the odd harmonics. At larger deformations, the viscous contribution increased, and non-linearities appeared. These outcomes indicated that OL formed a viscoelastic solid-like interfacial network, most likely due to non-covalent intermolecular interactions which disrupt at large deformations. The possible origins of these interactions between OL are discussed in the next section. In contrast, the PC-dominated interfaces (pure PC-stabilized interface and 1:3 OL-PC mixture) were fully elastic. The even harmonics had the main contribution to the non-linearity of the overall response, which suggested no or weak in-plane network interactions between PC molecules and a large contribution of density changes to the interfacial stress response. Our findings demonstrate that OL most likely contribute to the mechanics of the oleosome membrane by forming a solid-like interfacial network, while PC helps to reduce the interfacial tension (sections 3.1. and 3.2.1.).

In the next section, we will shortly discuss possible origins for the interfacial interactions between OL molecules and elaborate on how they might be important for the physical stability of oleosomes.

3.3. Discussion on the origin of the interactions between oleosins and their importance for the physical stability of oleosomes

When OL are adsorbed to the oil–water interface, their hydrophobic hairpin is supposed to be inserted into the oil phase [2,12,23]. The mostly hydrophilic arms are supposed to be positioned at the interface. The hairpin is solvated by the similarly highly hydrophobic oil phase; hence, we expect only weak intermolecular interactions between hairpins. The interfacial OL network is most likely based on non-covalent

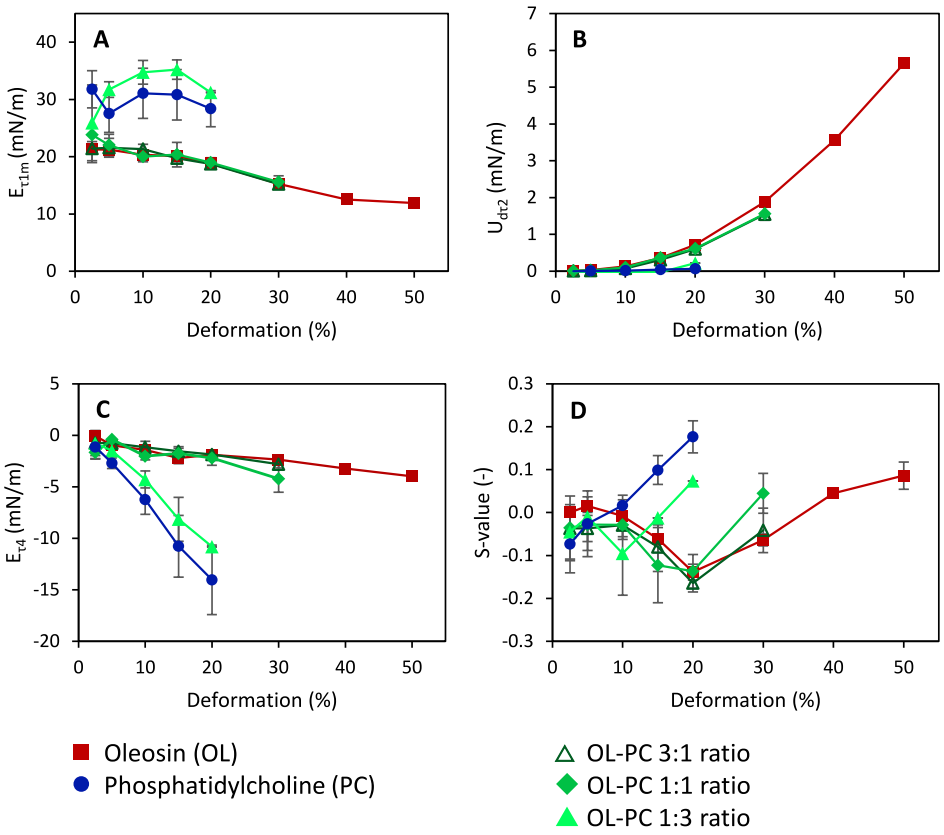

Fig. 5. $E_{\tau 1M}$ (A), U_{dt2} (B), $E_{\tau 4}$ (C) and Stiffening(S)-value (D) calculated from the general stress decomposition (GSD) of the rheological response by the oleosin (OL), phosphatidylcholine (PC) or the OL-PC mixture stabilized interfaces. The calculated parameters are plotted as a function of deformation. The ratios for the mixtures are shown as OL:PC(w:w).

interactions between the OL arms, in line with the previously observed destabilization of oleosomes after removing the OL arms enzymatically [47,48].

The OL network, and the so-formed viscoelastic solid-like interfacial film, are likely an important factor for the resistance of oleosomes against coalescence. This was demonstrated by the study of Nikolaou, et al. [49], which examined the coalescence stability of rapeseed oleosomes after exposing them to deformations during tribology measurements. The stability of the oleosomes was further compared to the stability of whey protein- or lecithin-stabilized oil droplets [49]. Whey proteins created a solid-like network at the droplet interfaces [25]. We expect a similar type of network for OL on the oleosome interfaces, considering that the OL:phospholipid ratio in rapeseed oleosomes is above 1:1 [30]. However, we must consider that both components will compete for the oil–water interface during the adsorption phase. As a result, the OL-to-PC ratio at the interface might differ from the one in the bulk solution. The gel-like networks stabilizing the whey droplets and the oleosomes appeared to prevent coalescence; both types of droplets remained largely intact after the deformation during the tribology measurements [49]. In contrast, the lecithin-stabilized droplets coalesced extensively during the measurements [49]. Lecithin is composed mostly of phospholipids that should not form a network when stabilizing the droplet interface, and this was reflected back in the stability of these droplets. Thus, we propose that the solid-like interfacial OL film provides the stability of oleosomes to coalescence. The phospholipids' function might be to further reduce the interfacial tension, which is particularly important during the formation of oleosomes by budding from the endoplasmic reticulum [26].

We recommend two attention points for future works. This work focuses on the main phospholipid, PC (60 % of the phospholipids on the membrane). Yet, the oleosomes membrane contains a rich mixture of phospholipids. The first recommendation is to study a mixture of phospholipids including all phospholipid classes of oleosomes. Such a study could yield further insights into the oleosome membrane as the anionic phospholipids present in oleosomes might have stronger electrostatic interactions with oleosins as the zwitterionic PC [50]. It should be considered that this electrostatic interaction might occur already in the bulk, which could influence the adsorption dynamics. Secondly, we recommend forcing droplets/interfacial films stabilized by OL and phospholipids into coalescence to confirm the suggested roles of both components further. Ideally, the interfacial concentrations should be measured or controlled to determine how much OL is needed to form the interfacial network that prevents coalescence.

4. Conclusions

In this study, we combined large amplitude dilatational oscillatory (LAOD) rheology with the new general stress decomposition (GSD) developed by de Groot, et al. [28] to study the mechanics of model oleosome interfaces. The outcomes illustrate how state-of-the-art interfacial science improves the understanding of oleosomes' physical stability. The possible roles of oleosins (OL) and phosphatidylcholines (PC) on the mechanical properties of the oleosome interface were identified, which marks a significant advancement over previously used techniques [15,51]. When solely OL stabilized the studied model oil–water interfaces, a viscoelastic solid-like interfacial network was formed, likely due to non-covalent intermolecular interactions between the adsorbed OL molecules. In contrast, the PC had weak in-plane interactions at the oil–water interface. In mixtures of 3:1 and 1:1 OL-PC, OL dominated the interfacial mechanics and formed a solid-like network, while the PC contributed to decreasing the interfacial tension. No interfacial network was formed for the 1:3 OL-PC ratio, where the PC dominated the

interfacial mechanics. In native oleosomes, the OL:phospholipid ratio is typically above 1:1 [32]. Therefore, we propose that OL dominate the interfacial mechanics in oleosomes. The interfacial OL film might be the origin of oleosomes' stability against coalescence, while the phospholipids appear to predominantly contribute by decreasing the interfacial tension.

The gained mechanistic understanding will help to introduce oleosomes as a "natural" alternative for emulsion applications in foods, cosmetics, and pharmaceuticals. Additionally, the understanding of oleosomes' design principles could enable the creation of bio-inspired droplets with uniquely high physical stability. As a final note, we highlight how the utilized GSD method allowed us to interpret the non-linear (dilatational) response of the interfacial films, which was essential to unravel the role of OL and PC at the interface. The presented toolset (LAOD & GSD) has great potential to provide a better understanding of other (biological) multi-component interfacial films.

CRediT authorship contribution statement

Jack Yang: Writing – original draft, Methodology, Investigation, Formal analysis, Conceptualization. **Lorenz Plankensteiner:** Writing – original draft, Methodology, Investigation, Formal analysis, Conceptualization. **Anteun de Groot:** Writing – original draft, Methodology, Investigation, Formal analysis. **Marie Hennebelle:** Writing – review & editing, Supervision, Conceptualization. **Leonard M.C. Sagis:** Writing – review & editing, Formal analysis, Supervision. **Constantinos V. Nikiforidis:** Writing – review & editing, Supervision, Conceptualization.

Declaration of competing interest

The authors declare that they have no known competing financial interests or personal relationships that could have appeared to influence the work reported in this paper.

Data availability

Data will be made available on request.

Acknowledgements

This research was partly funded by the Dutch Research Council (NWO) in the framework of the Green Top Sector Graduate School (GSGT.2019.021) and in collaboration with BOTANECO®.

Appendix A. Supplementary data

Supplementary data to this article can be found online at https://doi.org/10.1016/j.jcis.2024.09.171.

References

[1] D.J. Murphy, The biogenesis and functions of lipid bodies in animals, plants and microorganisms, Prog. Lipid Res. 40 (5) (2001) 325–438.
[2] J.T. Tzen, A.H. Huang, Surface structure and properties of plant seed oil bodies, J. Cell Biol. 117 (2) (1992) 327–335.
[3] A.R. Thiam, R.V. Farese Jr., T.C. Walther, The biophysics and cell biology of lipid droplets, Nat. Rev. Mol. Cell Biol. 14 (12) (2013) 775–786.
[4] D.J. Murphy, I. Hernández-Pinzón, K. Patel, Role of lipid bodies and lipid-body proteins in seeds and other tissues, J. Plant Physiol. 158 (4) (2001) 471–478.
[5] L. Rajjou, I. Debeaujon, Seed longevity: survival and maintenance of high germination ability of dry seeds, C. R. Biol. 331 (10) (2008) 796–805.
[6] C.V. Nikiforidis, Structure and functions of oleosomes (oil bodies), Adv. Colloid Interface Sci. 274 (2019) 102039.
[7] J. Weiss, H. Zhang, Recent advances in the composition, extraction and food applications of plant-derived oleosomes, Trends Food Sci. Technol. 106 (2020) 322–332.
[8] Z. Ma, J.H. Bitter, R.M. Boom, C.V. Nikiforidis, Thermal treatment improves the physical stability of hemp seed oleosomes during storage, LWT 189 (2023) 115551.
[9] P. Jolivet, C. Boulard, A. Bellamy, C. Larre, M. Barre, H. Rogniaux, S. d'Andrea, T. Chardot, N. Nesi, Protein composition of oil bodies from mature *Brassica napus* seeds, Proteomics 9 (12) (2009) 3268–3284.
[10] A.H. Huang, Plant lipid droplets and their associated proteins: potential for rapid advances, Plant Physiol. 176 (3) (2018) 1894–1918.
[11] A. Guzha, P. Whitehead, T. Ischebeck, K.D. Chapman, Lipid droplets: packing hydrophobic molecules within the aqueous cytoplasm, Annu. Rev. Plant Biol. 74 (2023) 195–223.
[12] J. Tzen, G. Lie, A. Huang, Characterization of the charged components and their topology on the surface of plant seed oil bodies, J Biol Chem 267 (22) (1992) 15626–15634.
[13] O. Leprince, A. Van Aelst, H. Pritchard, D. Murphy, Oleosins prevent oil-body coalescence during seed imbibition as suggested by a low-temperature scanning electron microscope study of desiccation-tolerant and-sensitive oilseeds, Planta 204 (1) (1997) 109–119.
[14] L. Plankensteiner, M. Hennebelle, J.-P. Vincken, C.V. Nikiforidis, Insights into the emulsification mechanism of the surfactant-like protein oleosin, J. Colloid Interface Sci. 657 (2023) 352–362.
[15] M. Deleu, G. Vaca-Medina, J.F. Fabre, J. Roiz, R. Valentin, Z. Mouloungui, Interfacial properties of oleosins and phospholipids from rapeseed for the stability of oil bodies in aqueous medium, Colloids Surf. BBiointerfaces 80 (2) (2010) 125–132.
[16] C.Y. Huang, A.H.C. Huang, Unique Motifs and Length of Hairpin in Oleosin Target the Cytosolic Side of Endoplasmic Reticulum and Budding Lipid Droplet, Plant Physiol. 174 (4) (2017) 2248–2260.
[17] C.C. Peng, I.P. Lin, C.K. Lin, J.T. Tzen, Size and stability of reconstituted sesame oil bodies, Biotechnol. Prog. 19 (5) (2003) 1623–1626.
[18] A.J. Board, J.M. Crowther, A. Acevedo-Fani, C.-N. Meisrimler, G.B. Jameson, R.C. Dobson, How plants solubilise seed fats: revisiting oleosin structure and function to inform commercial applications, Biophysical Reviews (14(1)) (2022) 257-266.
[19] J.A. Julien, S.G. Mutchek, N.J. Wittenberg, K.J. Glover, Biophysical characterization of full-length oleosin in dodecylphosphocholine micelles, Proteins 90 (2) (2022) 560–565.
[20] M. Li, J.S. Keddie, L.J. Smith, D.C. Clark, D.J. Murphy, Expression and characterization of the N-terminal domain of an oleosin protein from sunflower, J Biol Chem 268 (23) (1993) 17504–17512.
[21] J. Jumper, R. Evans, A. Pritzel, T. Green, M. Figurnov, O. Ronneberger, K. Tunyasuvunakool, R. Bates, A. Zidek, A. Potapenko, A. Bridgland, C. Meyer, S.A. A. Kohl, A.J. Ballard, A. Cowie, B. Romera-Paredes, S. Nikolov, R. Jain, J. Adler, T. Back, S. Petersen, D. Reiman, E. Clancy, M. Zielinski, M. Steinegger, M. Pacholska, T. Berghammer, S. Bodenstein, D. Silver, O. Vinyals, A.W. Senior, K. Kavukcuoglu, P. Kohli, D. Hassabis, Highly accurate protein structure prediction with AlphaFold, Nature 596 (7873) (2021) 583–589.
[22] M.D. Huang, A.H. Huang, Bioinformatics Reveal Five Lineages of Oleosins and the Mechanism of Lineage Evolution Related to Structure/Function from Green Algae to Seed Plants, Plant Physiol. 169 (1) (2015) 453–470.
[23] P. Jolivet, L. Ayme, A. Giuliani, F. Wien, T. Chardot, Y. Gohon, Structural proteomics: Topology and relative accessibility of plant lipid droplet associated proteins, J. Proteomics 169 (2017) 87–98.
[24] D.J. McClements, L. Bai, C. Chung, Recent Advances in the Utilization of Natural Emulsifiers to Form and Stabilize Emulsions, Annual Reviews in Food, Sci. Technol. 8 (2017) 205–236.
[25] E.B. Hinderink, L. Sagis, K. Schroën, C.C. Berton-Carabin, Behavior of plant-dairy protein blends at air-water and oil-water interfaces, Colloids Surf. B Biointerfaces 192 (2020) 111015.
[26] K. Ben M'barek, D. Ajjaji, A. Chorlay, S. Vanni, L. Foret, A.R. Thiam, ER Membrane Phospholipids and Surface Tension Control Cellular Lipid Droplet Formation, Developmental Cell 41(6) (2017) 591-604 e7.
[27] L.M. Sagis, P. Fischer, Nonlinear rheology of complex fluid–fluid interfaces, Curr. Opin. Colloid Interface Sci. 19 (6) (2014) 520–529.
[28] A. de Groot, J. Yang, L.M.C. Sagis, Surface stress decomposition in large amplitude oscillatory interfacial dilatation of complex interfaces, J. Colloid Interface Sci. 638 (2023) 569–581.
[29] L.M. Sagis, E. Scholten, Complex interfaces in food: Structure and mechanical properties, Trends Food Sci. Technol. 37 (1) (2014) 59–71.
[30] C. Boulard, M. Bardet, T. Chardot, B. Dubreucq, M. Gromova, A. Guillermo, M. Miquel, N. Nesi, S. Yen-Nicolaÿ, P. Jolivet, The structural organization of seed oil bodies could explain the contrasted oil extractability observed in two rapeseed genotypes, Planta 242 (1) (2015) 53–68.
[31] L. Plankensteiner, J. Yang, J.H. Bitter, J.-P. Vincken, M. Hennebelle, C. Nikiforidis, High yield extraction of oleosins, the proteins that plants developed to stabilize oil droplets, Food Hydrocoll. 137 (2022) 108419.
[32] J. Tzen, Y. Cao, P. Laurent, C. Ratnayake, A. Huang, Lipids, Proteins, and Structure of Seed Oil Bodies from Diverse Species, Plant Physiol. 101 (1) (1993) 267–276.
[33] J. Bergfreund, P. Bertsch, P. Fischer, Adsorption of proteins to fluid interfaces: Role of the hydrophobic subphase, J. Colloid Interface Sci. 584 (2021) 411–417.
[34] R. Zhang, P. Somasundaran, Advances in adsorption of surfactants and their mixtures at solid/solution interfaces, Adv. Colloid Interface Sci. 123 (2006) 213–229.
[35] C.V. Kulkarni, Lipid crystallization: from self-assembly to hierarchical and biological ordering, Nanoscale 4 (19) (2012) 5779–5791.
[36] R. Mezzenga, J.M. Seddon, C.J. Drummond, B.J. Boyd, G.E. Schroder-Turk, L. Sagalowicz, Nature-Inspired Design and Application of Lipidic Lyotropic Liquid Crystals, Adv. Mater. 31 (35) (2019) e1900818.

[37] L. Lei, Y. Ma, D.R. Kodali, J. Liang, H.T. Davis, Ternary phase diagram of soybean phosphatidylcholine-water-soybean oil and its application to the water degumming process, J. Am. Oil Chem. Soc. 80 (4) (2003) 383–388.
[38] Y. Gohon, J.D. Vindigni, A. Pallier, F. Wien, H. Celia, A. Giuliani, C. Tribet, T. Chardot, P. Briozzo, High water solubility and fold in amphipols of proteins with large hydrophobic regions: oleosins and caleosin from seed lipid bodies, BBA 1808 (3) (2011) 706–716.
[39] K.B. Vargo, R. Parthasarathy, D.A. Hammer, Self-assembly of tunable protein suprastructures from recombinant oleosin, Proceedings of the National Academy of Sciences 109(29) (2012) 11657-62.
[40] R. Pichot, R.L. Watson, I.T. Norton, Phospholipids at the interface: current trends and challenges, Int. J. Mol. Sci. 14 (6) (2013) 11767–11794.
[41] W. Xia, T.E. Botma, L.M. Sagis, J. Yang, Selective proteolysis of β-conglycinin as a tool to increase air-water interface and foam stabilising properties of soy proteins, Food Hydrocoll. 130 (2022) 107726.
[42] J. Yang, L.C. Waardenburg, C.C. Berton-Carabin, C.V. Nikiforidis, E. van der Linden, L.M.C. Sagis, Air-water interfacial behaviour of whey protein and rapeseed oleosome mixtures, J. Colloid Interface Sci. 602 (2021) 207–221.
[43] R.H. Ewoldt, A. Hosoi, G.H. McKinley, New measures for characterizing nonlinear viscoelasticity in large amplitude oscillatory shear, J. Rheol. 52 (6) (2008) 1427–1458.
[44] L.M. Sagis, K.N. Humblet-Hua, S.E. van Kempen, Nonlinear stress deformation behavior of interfaces stabilized by food-based ingredients, J. Phys. Condens. Matter 26 (46) (2014) 464105.
[45] E. Dickinson, Y. Matsumura, Time-dependent polymerization of β-lactoglobulin through disulphide bonds at the oil-water interface in emulsions, Int. J. Biol. Macromol. 13 (1) (1991) 26–30.
[46] J. Yang, P. Shen, A. de Groot, H.C.M. Mocking-Bode, C.V. Nikiforidis, L.M.C. Sagis, Oil-water interface and emulsion stabilising properties of rapeseed proteins napin and cruciferin studied by nonlinear surface rheology, J. Colloid Interface Sci. 662 (2024) 192–207.
[47] S. Maurer, G. Waschatko, D. Schach, B.I. Zielbauer, J. Dahl, T. Weidner, M. Bonn, T.A. Vilgis, The role of intact oleosin for stabilization and function of oleosomes, J. Phys. Chem. B 117 (44) (2013) 13872–13883.
[48] M. Li, D.J. Murphy, K.H. Lee, R. Wilson, L.J. Smith, D.C. Clark, J.Y. Sung, Purification and structural characterization of the central hydrophobic domain of oleosin, J Biol Chem 277 (40) (2002) 37888–37895.
[49] F. Nikolaou, J. Yang, L. Ji, E. Scholten, C.V. Nikiforidis, The role of membrane components on the oleosome lubrication properties, J. Colloid Interface Sci. 657 (2024) 695–704.
[50] C. Bourgeois, A.I. Gomaa, T. Lefevre, M. Cansell, M. Subirade, Interaction of oil bodies proteins with phospholipid bilayers: A molecular level elucidation as revealed by infrared spectroscopy, Int. J. Biol. Macromol. 122 (2019) 873–881.
[51] E. Roux, S. Baumberger, M.A. Axelos, T. Chardot, Oleosins of Arabidopsis thaliana: expression in Escherichia coli, purification, and functional properties, J. Agric. Food Chem. 52 (16) (2004) 5245–5249.